Electronic Supplementary Material (ESI) for Polymer Chemistry.

SUPPORTING INFORMATION

Predicting the orientation of magnetic microgel rods for soft anisotropic biomimetic hydrogels

Jonas C. Rose, Maaike Fölster, Lukas Kivilip, Jose L. Gerardo-Nava, Esther E. Jaekel, David B. Gehlen, Wilko Rohlfs, Laura De Laporte**

Supplementary Explanations

The mechanism, which causes the rod-shaped microgels (consisting of a crosslinked polymer matrix material with a small volume fraction of SPIONs, approx. 10^{-3} vol-%) to align in a magnetic field is explained in the following paragraph. The embedded SPIONs can be seen as dipoles, i.e. single domain magnetic particles of spherical shape, which magnetize in the presence of an external field (H0). The dipole moment $\vec{m}$ of each SPION is given by Equation 1 (E1) and induces a magnetic field in the vicinity of the SPIONs (see Figure 2A), described by:

$$\vec{H}_{\text{dipole}}(\vec{r}) = \frac{1}{4\pi}\left(3\frac{\vec{r}(\vec{m}\cdot\vec{r})}{r^5} - \frac{\vec{m}}{r^3}\right) \quad \text{(SE1)}$$

where the vector $\vec{r}$ originates in the dipole. Obviously, the magnetic field decays by H_i dipole $\propto 1/r^3$

Inside the microgel, the SPIONs interact with the external magnetic field as well as with each other due to the local change in the magnetic field. This in turn influences the magnitude of magnetization as well as the orientation of the SPIONs (right picture in Figure 2B, 2C). Thus, the total magnetic field is given by the external field H_0 and the superposition of all magnetic fields created by the SPIONs.

$$\vec{H}(\vec{r}) = \vec{H}_0 + \sum_{SPIONs} \vec{H}_i(\vec{m}_i, \vec{r}_i) \quad \text{(SE2)}$$

Note that the back coupling with Equation 4 requires an iterative procedure to calculate the magnetic field, especially if the magnetization is described by a more complex function.

Each dipole in the magnetic field is subject to a force

$$\vec{F} = \mu \cdot \nabla(\vec{m} \cdot \vec{H}) \tag{SE3}$$

where ∇ denotes the gradient operator. Note, as the magnetization $\vec{m}$ is assumed to be constant throughout the single domain magnetic particle, a force is only present in an inhomogeneous magnetic field. This is obviously the case in the microgel as seen in Figure S2. The sum of forces on all SPIONs in a non-spherical microgel cause a torque

$$\vec{T} = \sum_{\text{SPIONs}} \vec{s}_i \times \vec{F}_i \tag{SE4}$$

where si is the distance from the SPION to the center of rotation. The magnetic torque is the driving force for the rotation of the microgel and balanced by viscous forces.

The Model: The physical explanations provided in the previous paragraph are grounded on the magnetic response of single SPIONs in the magnetic field. In order to model the rotation of microgels with a larger number of SPIONs, an integral model is desired, which accounts for the main physical mechanisms and that can predict the orientation rate depending on the microgel and external parameters. In the present study, a model for the rotation of homogeneous ellipsoids in magnetic field is adapted.[18, 19]

The model grounds on the balance between magnetic torque, T_M, and viscous torque, T_v, and is thus applicable for small particles where inertia is negligible. In this case, the sum of the two forces must vanish, i.e. $T_M + T_v = 0$.

The viscous torque on an axisymmetric element in a motionless unbounded Newtonian fluid under Stokes flow conditions is given by[19, 34]

$$T_v = -f_r \eta \Omega \tag{SE5}$$

where η denotes the viscosity of the surrounding liquid, Ω is the angular velocity, and f_r is the rotational frictional coefficient. The latter only depends on the geometrical parameters of the rotating ellipsoid. For a prolate ellipsoid (football-shaped) the half-lengths of the long axis is denoted by a and the half-lengths of the two other axes by b. As such, the form coefficient is given by p = a/b and larger than one. The volume of this ellipsoid is $V_{ellipsoid} = (4/3)\pi ab^2$. According to Perrin's work[35] the rotational frictional coefficient for this object is.[36]

$$f_r = 8\pi a b^2 \frac{4\left(1-q^4\right)}{3q^2\left(S\left(2-q^2\right)-2\right)} \tag{SE6}$$

where q is the inverse of the form factor q = (1/p), and S is defined by

$$S = \frac{2}{\sqrt{1-q^2}} \ln\left(\frac{1+\sqrt{1-q^2}}{q}\right) \tag{SE7}$$

Note that Equation SE6 can be divided by the volume of the ellipsoid showing that the volume specific friction coefficient does not depend on the actual size of the ellipsoid but only upon the aspect ratio.

First experimental results show a saturating behavior of the rotation rate with increasing magnetic field strength above 40 mT. This indicates the importance of the non-linear magnetization behavior with a saturation for high magnetic field strength. Thus, linear models for the magnetization as for instance used in[11, 20, 31] cannot be applied. For a general model with non-linear magnetization behavior (including saturation), the equations presented in Shine and Armstrong are used.[18] However, it

should be noted that these equations are valid only for a material with homogeneous material properties. The magnetic torque is then given by

$$T_{\mathrm{M}} = V_{\mathrm{ellipsoid}} \frac{\mu_0 H_0^2 M^2 \left(D_{\mathrm{yy}} - D_{\mathrm{xx}}\right) sin\beta cos\beta}{\left(H_{\mathrm{i}} + D_{\mathrm{xx}} M\right)\left(H_{\mathrm{i}} + D_{\mathrm{yy}} M\right)} \quad \text{(SE8)}$$

In this equation, the magnitude of the external magnetic field H0 and the internal magnetic field H_i are of importance.

For a homogeneous ellipsoid located in a uniform, parallel external field, the solution of Maxwell's equations (Equation SE12) reveal that H_i is uniform. For more details on the derivation of the equation we refer to the before mentioned publication.

The internal field is determined by are constant throughout the volume of the ellipsoid.

$$\vec{H}_{\mathrm{i}} = \vec{H}_0 - D \cdot \vec{M} \quad \text{(SE9)}$$

where D denotes the demagnetization tensor. For an ellipsoidal object, these diagonal values of D are

$$D_{\mathrm{xx}} = 1 - A, D_{\mathrm{yy}} = D_{\mathrm{zz}} = A/2 \quad \text{(SE10)}$$

and A is given by

$$A = \frac{p^2}{p^2 - 1} - \frac{p cos^{-1}(p)}{(p^2 - 1)^{2/3}} \quad \text{(SE11)}$$

Note that the quantities $\vec{H}_i$ and $\vec{M}$ are not explicitly known because they are coupled with the non-linear magnetization function $M_{\mathrm{i}}(H_{\mathrm{i}})$.

In contrast to the ellipsoid, the internal magnetic field of the more heterogeneous microgels is varying within the microgel and depends on the microgel dimensions and shape, the SPION distribution inside the microgel, and the strength of the external

magnetic field. Therefore, a critical issue in this model is the calculation of the internal magnetic field and its variation due to the demagnetization tensor. If a volume average value for the magnetization of the material M is used in Equation SE12, the second term on the right hand side becomes negligible. However, experimental results in Figure 2E demonstrate a strong asymmetry of the curves, suggesting that demagnetization has a severe influence. The reason for this demagnetization may be the strong magnetic field around each SPION that affects the neighboring SPIONs. A physically motivated description of this interaction is missing. To overcome this critical issue, a third coefficient is introduced in the model that accounts for the higher influence of demagnetization. Thus, equation SE12 is rewritten to

$$\vec{H}_i = \vec{H}_0 - C_{\text{demag}} D \cdot \vec{M} \qquad \text{(SE12)}$$

where C_{demag} is a model parameter.

Rod-shaped particles vs. ellipsoidal particles: Under the experimental conditions, performed in this report, rod-shaped microgels with a square cross-section are applied, whereas the model assumes ellipsoidal particles for the demagnetization tensor D_{ii} and the rotational frictional coefficient.[35] This assumption is necessary because only for an ellipsoid, the Maxwell equations in an unbounded, uniform, parallel external field[18] yields a uniform and parallel internal magnetic field Hi. For the case of a cylinder with a circular or square cross-section, the internal magnetic field becomes non-uniform, which significantly increases the complexity of the modeling approach. Therefore, it is convenient for a quantitative analysis to treat the microgel as a long prolate ellipsoid.[37] However, differences in the geometry need to be considered in future numerical studies.

Estimating the apparent microgel magnetization: In order to estimate the apparent microgel magnetization for a specific dataset, the apparent magnetization, M (H_i) and internal magnetic field intensity H_i are determined by fitting the experimental data as shown in Figure S5. Note, that the experimental data points (angle dependent rotation speed) of each tracked microgel are clustered into intervals (5 deg) and the median value of each interval is utilized. The apparent microgel magnetization is approximated by a fifth-degree polynomial fit. Above a magnetic field of 80,000A/m, the magnetization is assumed to take a constant value.

In a second step, the model parameters of the polynomial fit and the correction factor for demagnetization C_{demag} are subjected to an optimization algorithm using the same input data. This optimization reduces the difference between the experimental rotation velocity and the predicted velocity by varying the model constants.

Supplementary Figures

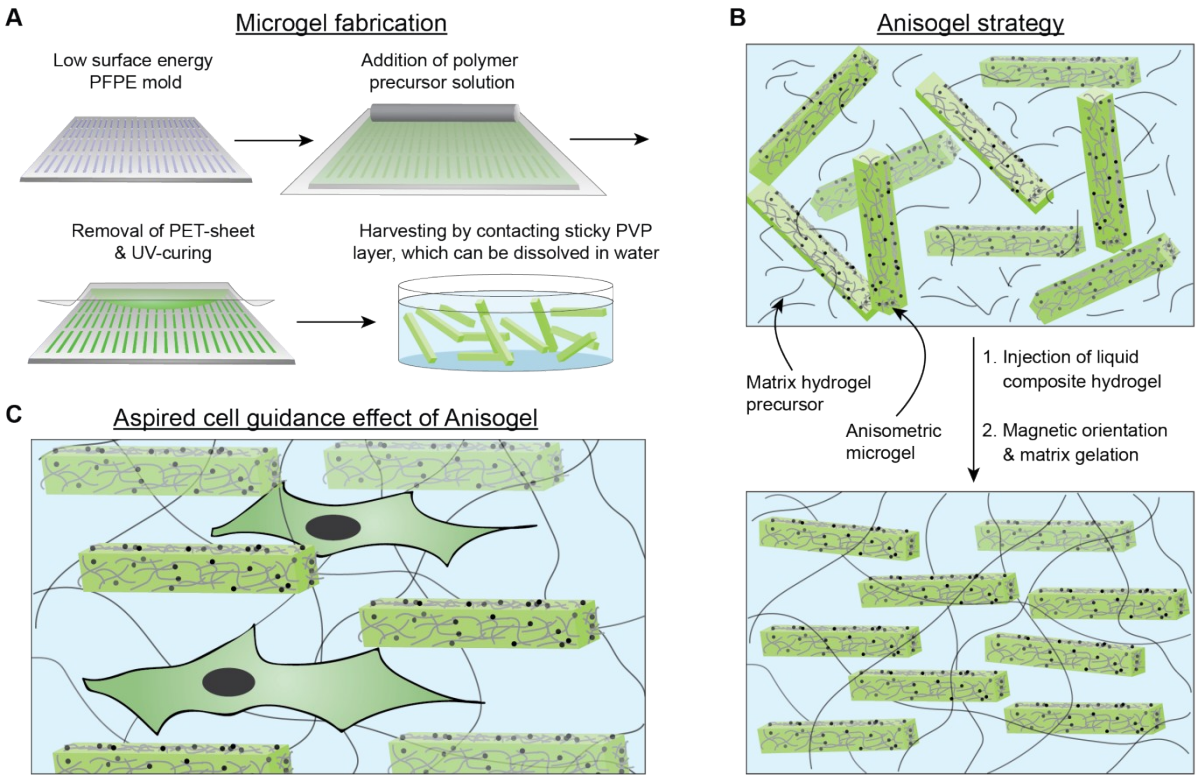

Figure S1: A) Soft microgels are fabricated via a mold-based soft lithography approach, which is adapted from the PRINT technique. This involves casting perfluoropolyether (PFPE) or polydimethylsiloxane (PDMS) on a patterned wafer to produce a repelling mold. Afterward, the microgel precursor solution is spread on top and captured within the mold cavities. After polymerization, the microgels are retrieved by a sticky water-soluble polyvinylpyrrolidone (PVP) glue layer. B) The Anisogel strategy comprises of dispersing the microgels, which are loaded with SPIONs, inside an in situ crosslinking pre-polymer solution. After injection, the microgels are aligned and their position and orientation are fixed by the surrounding hydrogel matrix. C) The microgels create an anisotropy, which the cells sense, triggering their decision to grow aligned.

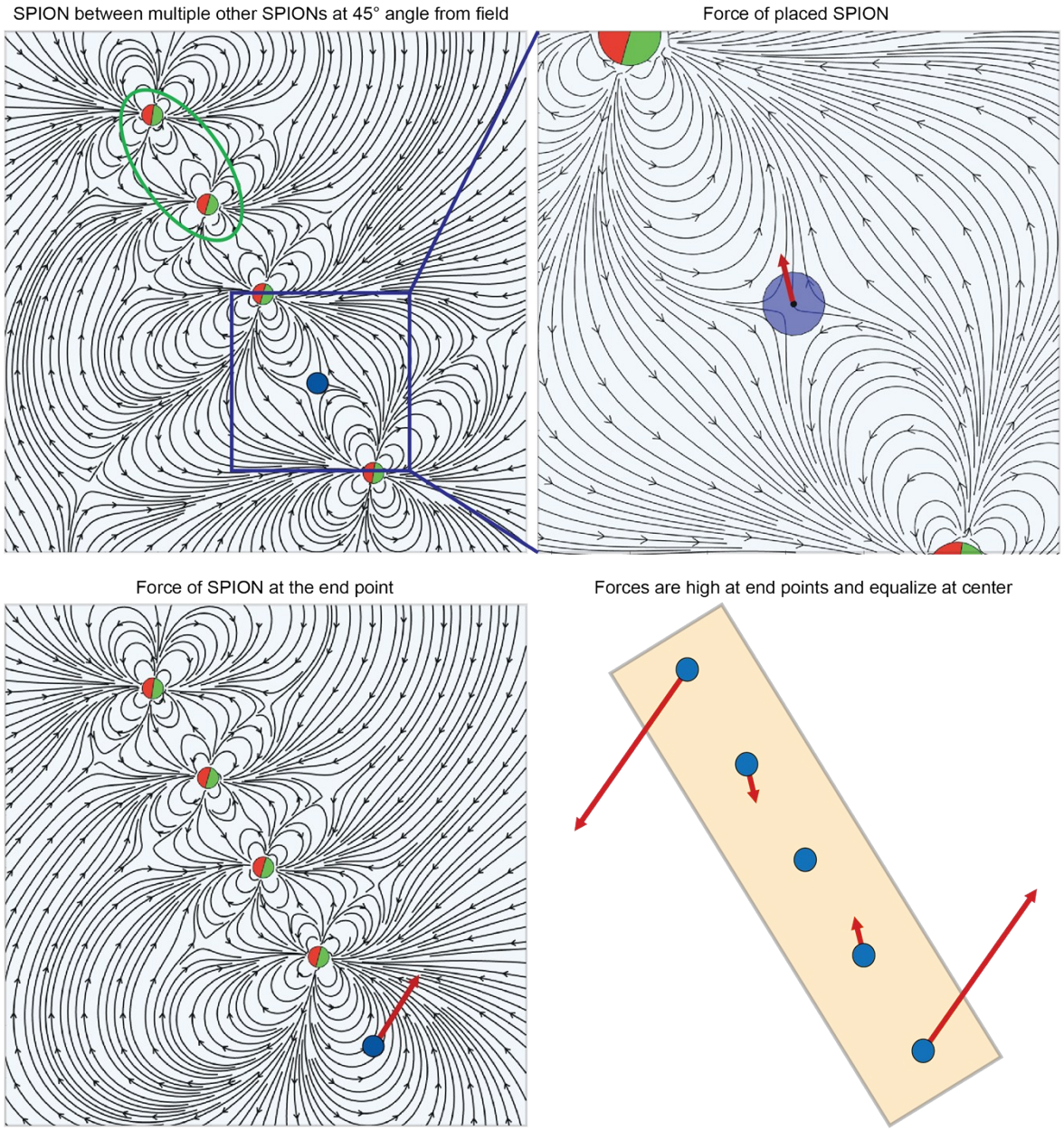

Figure S2: Local magnetic field lines and exerted forces by multiple SPIONs ordered in a row in a 45◦ angle with regard to the external field. High aspect ratios lead to increasing forces (red arrows) at the ends of the rectangular geometries of the microgels, as the magnetic dipole moments are not symmetrically stabilized by the surrounding SPIONs. In contrast, SPIONs in the middle of the chain do not exert a force.

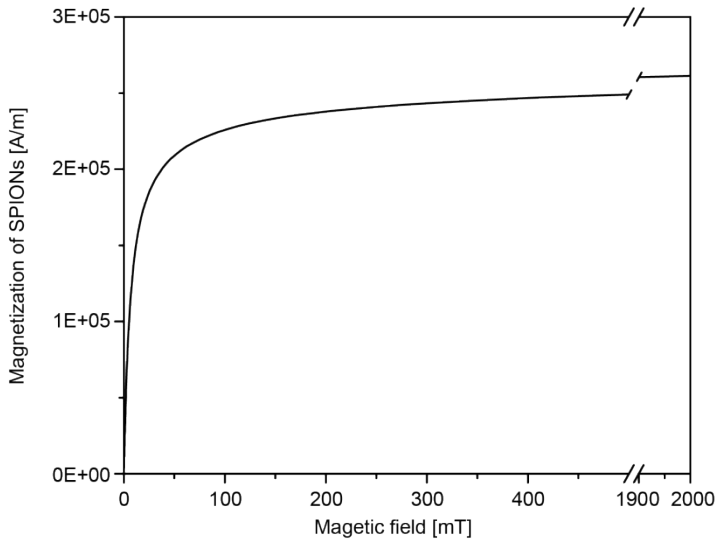

Figure S3: Magnetization of 100% EMG-700 SPIONs in dependence of magnetic field strength. Kindly provided by Ferrotec (USA) Corporation.

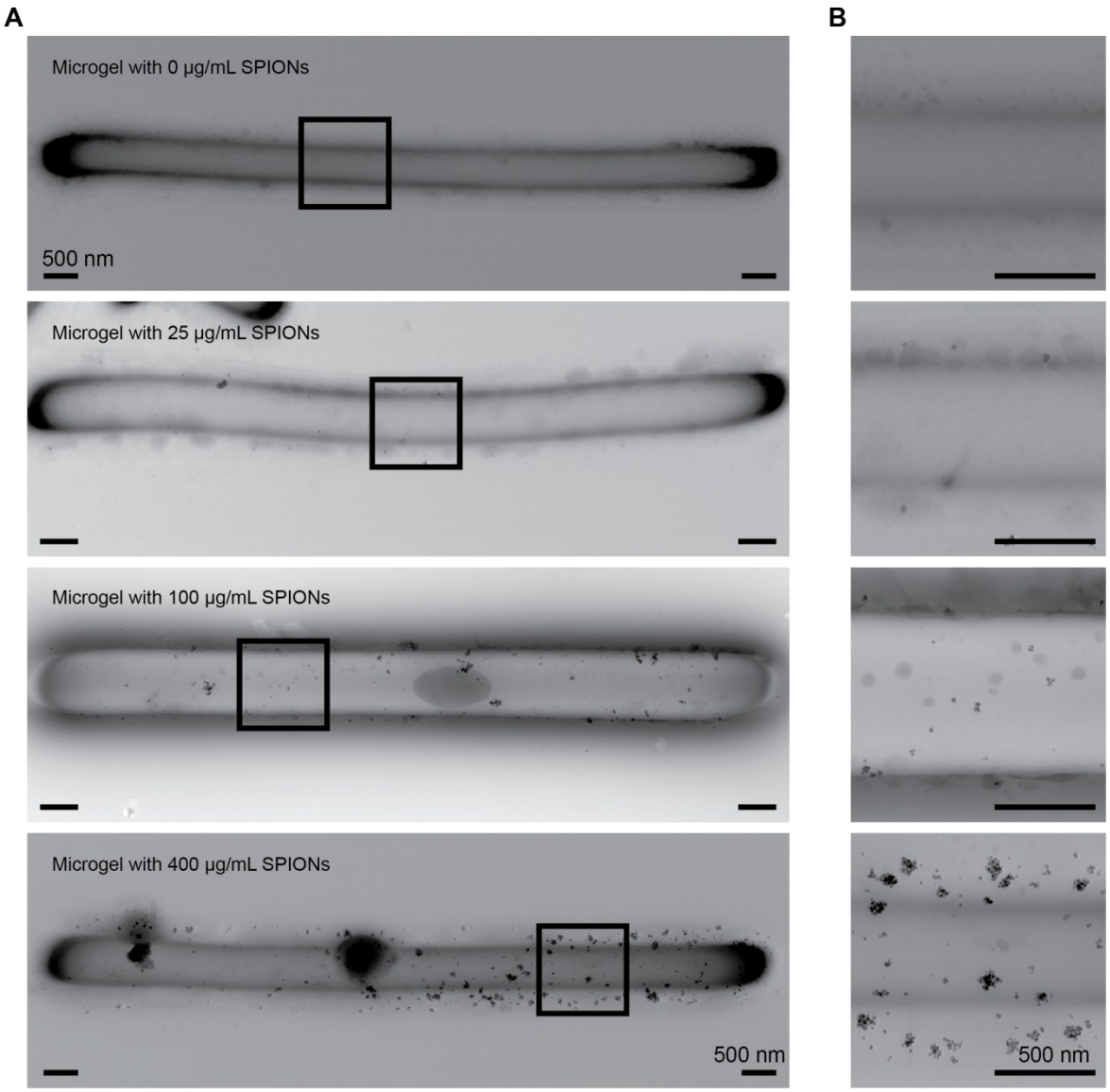

Figure S4: (A) STEM-images of representative microgels containing different amounts of SPIONs (0, 25, 100, or 400 µg/mL). (B) Magnifications of microgels depicted in A (black box). The STEM-images do not resolve spatially, which leads to visually closer appearing SPIONs. Noteworthy, the contours do not represent the actual microgel geometries, as microgels collapse upon drying.

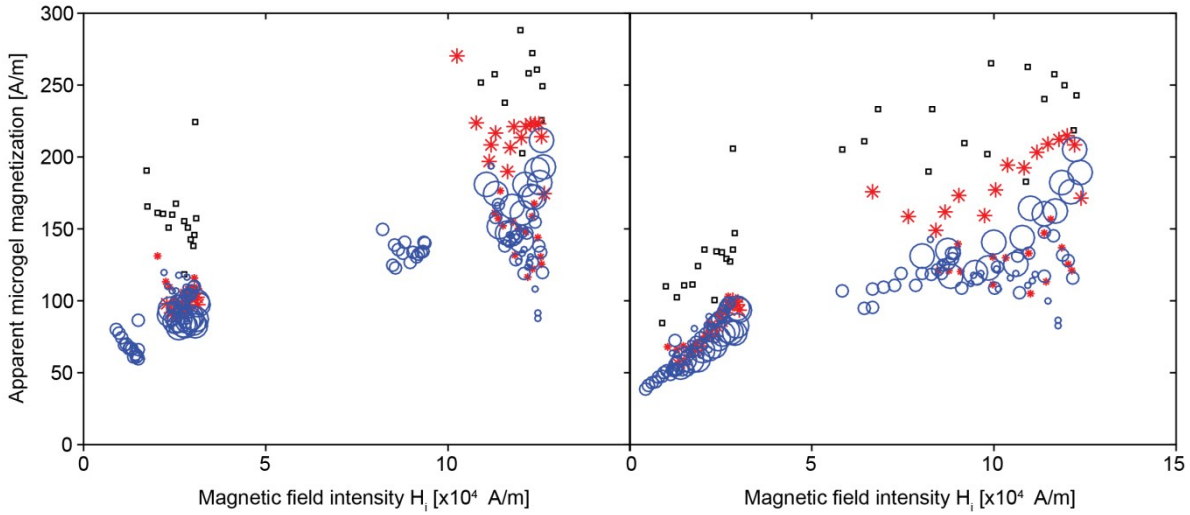

Figure S5: Apparent material magnetization versus the magnetic field intensity for different microgel sizes with a diameter of 10 µm (blue), 2.5 µm (black), and 5 µm (red). The aspect ratio scales with symbol size; for a diameter of 10 µm, aspect ratios ranging between 2.5 and 20 are tested. Two demagnetization parameters are compared, C_{demag}: 200 or 800.

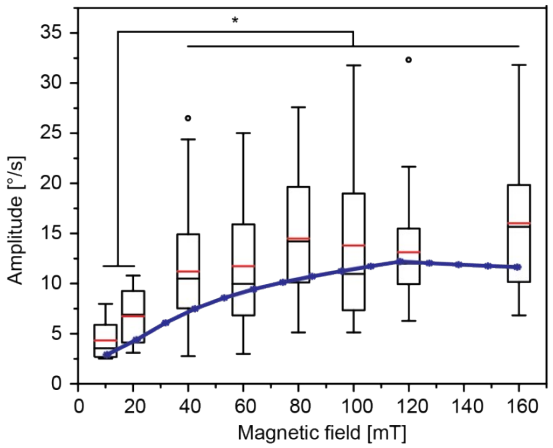

Figure S6: Amplitudes of microgel orientation for a size of 10 · 10 · 50 µm3 supplemented with SPION contents of 400 µg/mL in different magnetic fields ranging from 10 to 160 mT. The modeled amplitudes are depicted as the blue curve.

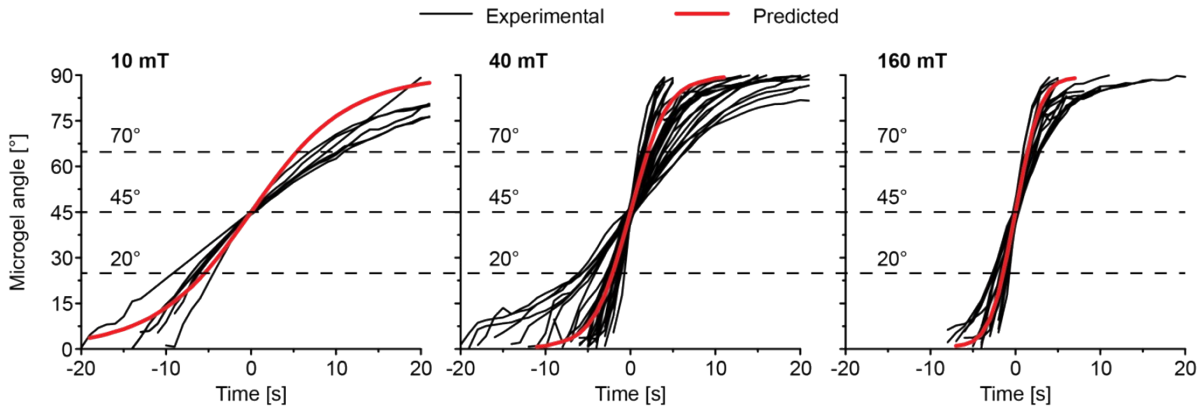

Figure S7: Comparison of the calculated (red) and experimental (black) orientation over time for different magnetic fields (10, 40, 160 mT). An angle of 45° is set as the starting point (t = 0 s).

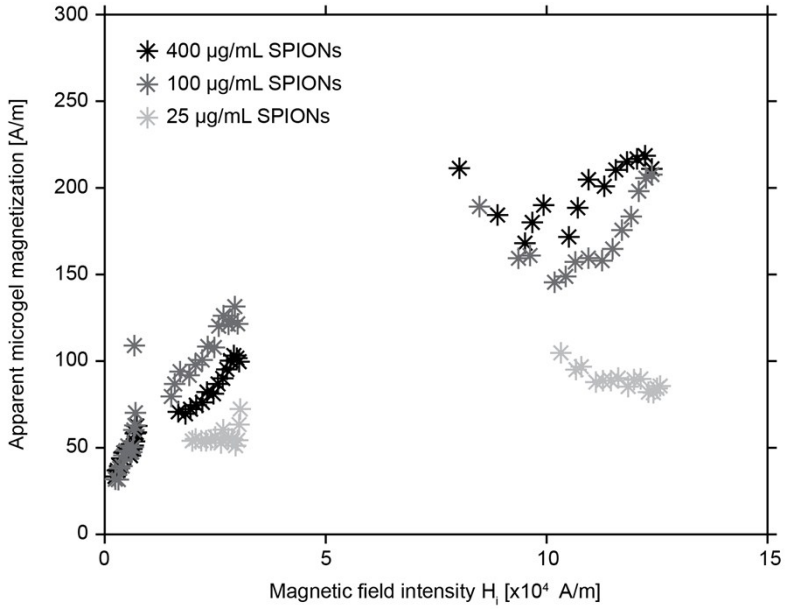

Figure S8: Apparent material magnetization versus the magnetic field intensity for microgels with a size of 5 · 5 · 50 µm³ and different SPION contents. The plot reveals differences in the apparent magnetization in function of the internal magnetic field (C_{demag} = 500). While the apparent magnetization roughly doubles from 25 µg/mL (light grey) to 100 µg/mL (dark grey) at H_0 = 40 and 120 mT, the increase to 400 µg/mL (black) only leads to slightly higher apparent microgel magnetization at 120 mT.

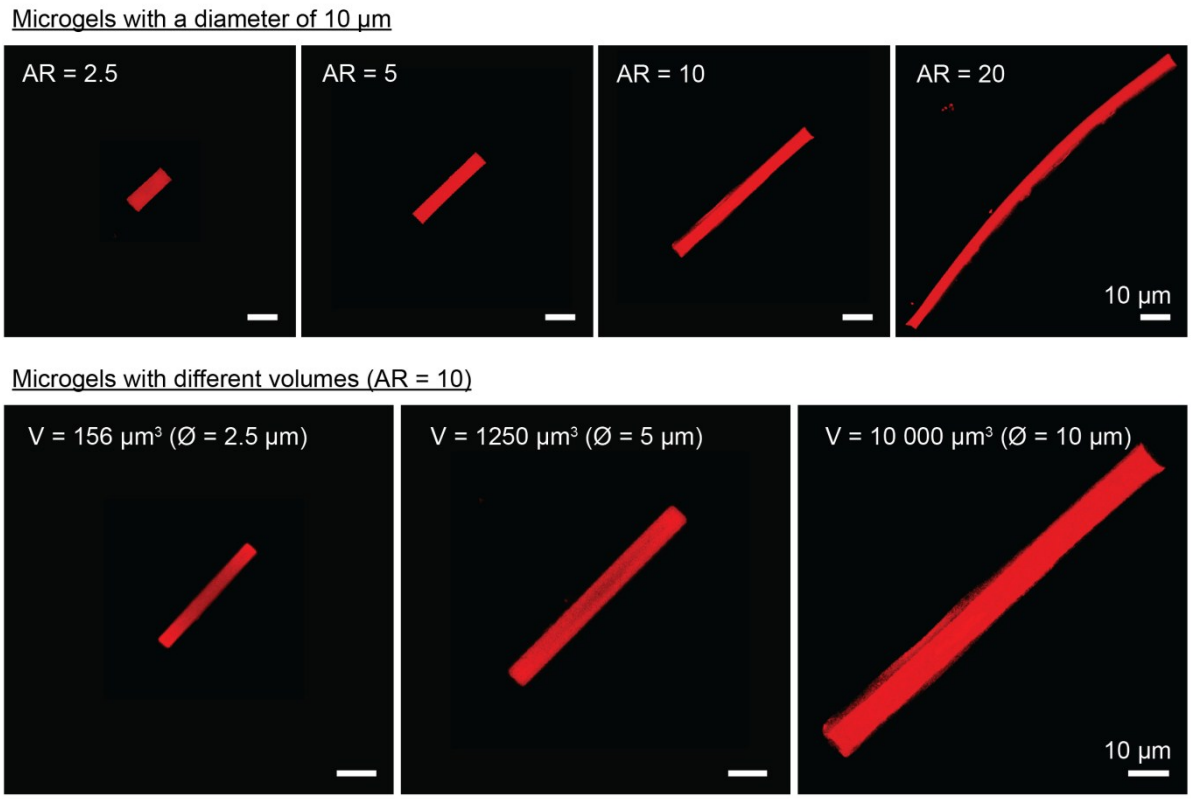

Figure S9: Confocal images of microgels that are applied for analysis. Microgels are varied in their aspect ratio (AR) and volume.

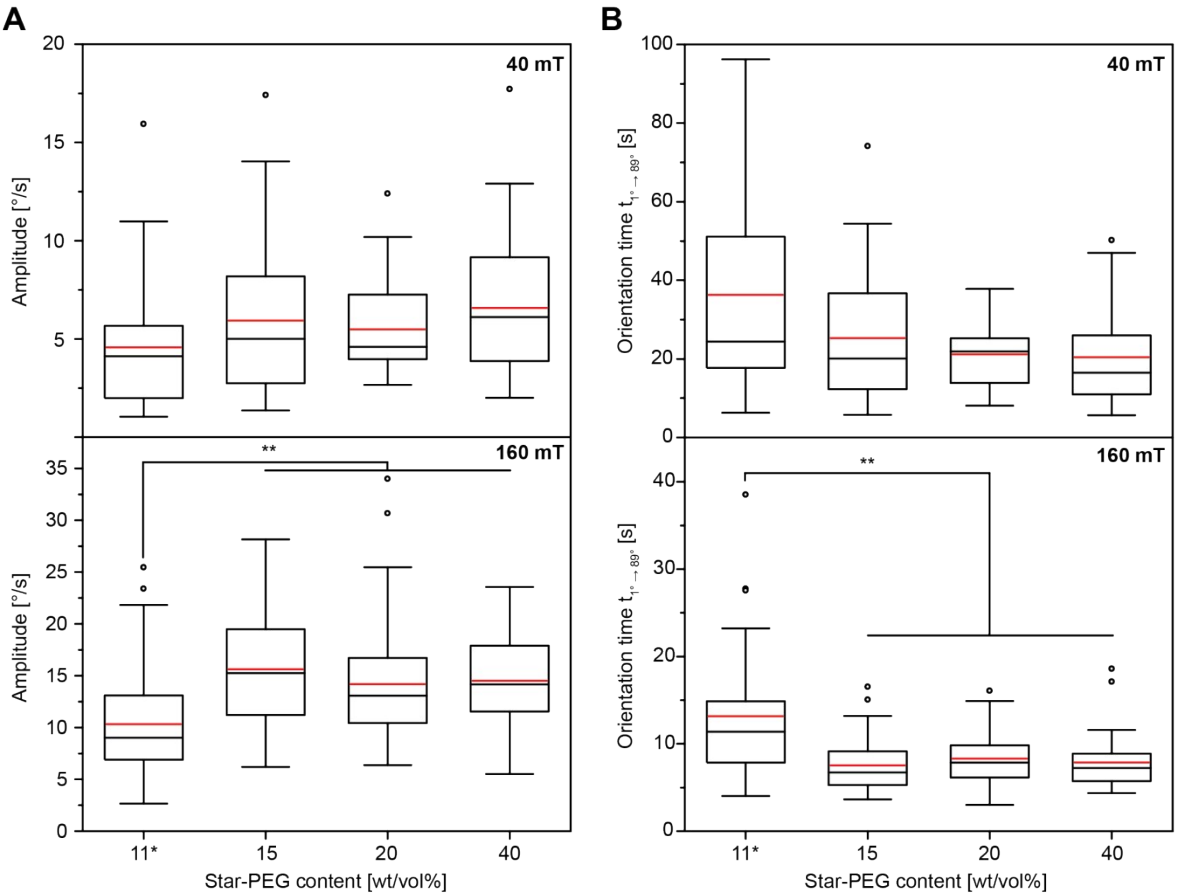

Figure S10: Amplitude (A) and orientation time (B) of microgels fabricated with different polymer contents (11 wt/vol% 25/75 star-PEG-acrylate/PEG-diacrylate, 15, 20, and 40 wt/vol% star-PEG-acrylate), which result in different stiffness. Two different magnetic fields of 40 and 160 mT are applied.

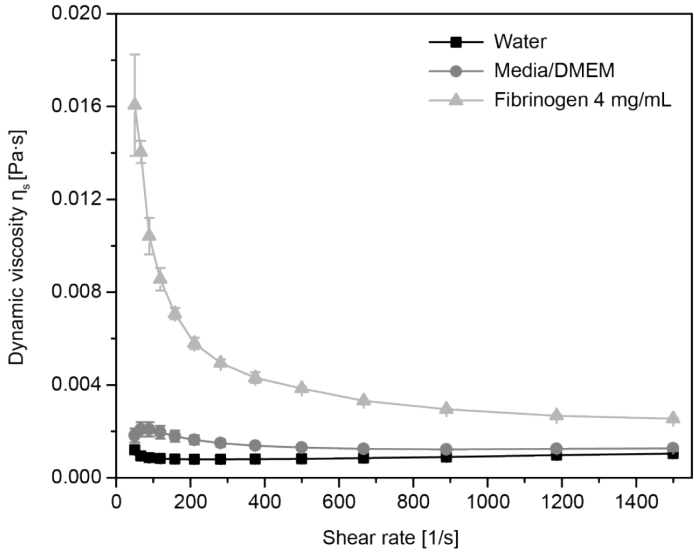

Figure S11: Dynamic viscosity of water, cell culture media (DMEM), and fibrinogen in DMEM (4 mg/mL) in dependence of the shear rate.

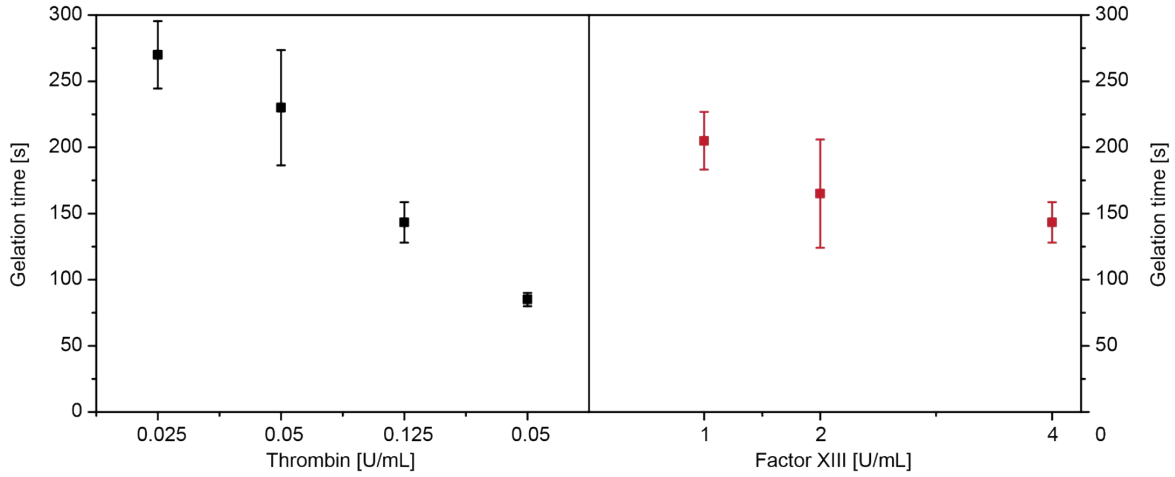

Figure S12: The gelation kinetics of fibrin are varied by the concentration of thrombin (constant factor XIII concentration of 4 U/mL) or factor XIII (constant thrombin concentration of 0.125 U/mL) to adapt for different microgel orientation times.

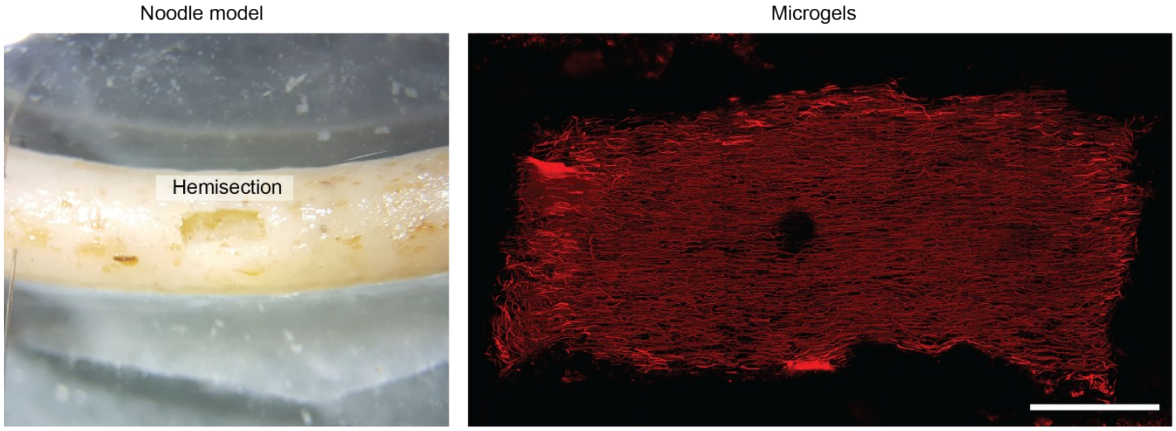

Figure S13: Model for spinal cord hemisection. The hemisection is cut into a well-cooked spaghetti noodle, which is placed next to a 1 cm^3 rare earth magnet. Inside the cavity of the hemisection, microgels of 2.5 · 2.5 · 50 μm^3 and 400 µg/mL SPIONs are co-injected with a fibrinogen-enzyme mixture. Microgels are imaged by confocal microscopy with a z-depth of 500 µm. Scale bar is 500 µm.